Research Article

Journal of Molecular Microbiology and Biotechnology

J Mol Microbiol Biotechnol 2015;25:178–194
DOI: 10.1159/000381214

Published online: July 9, 2015

Modeling the Interplay of *Pseudomonas putida* EIIA^{Ntr} with the Potassium Transporter KdpFABC

S. Wolf K. Pflüger-Grau A. Kremling

FG Systems Biotechnology, Technische Universität München, Garching, Germany

Key Words
Nitrogen phosphotransferase system · Two-component system · KdpFABC potassium transporter

Abstract
The nitrogen phosphotransferase system (PTS^{Ntr}) of *Pseudomonas putida* is a key regulatory device that participates in controlling many physiological processes in a posttranscriptional fashion. One of the target functions of the PTS^{Ntr} is the regulation of potassium transport. This is mediated by the direct interaction of one of its components with the sensor kinase KdpD of the two-component system controlling transcription of the *kdpFABC* genes. From a detailed experimental analysis of the activity of the *kdpF* promoter in *P. putida* wild-type and *pts* mutant strains with varying potassium concentrations, we had highly time-resolved data at hand, describing the influence of the PTS^{Ntr} on the transcription of the KdpFABC potassium transporter. Here, this data was used to construct a mathematical model based on a black box approach. The model was able to describe the data quantitatively with convincing accuracy. The qualitative interpretation of the model allowed the prediction of two general points describing the interplay between the PTS^{Ntr} and the KdpFABC potassium transporter: (1) the influence of cell number on the performance of the *kdpF* promoter is mainly by dilution by growth and (2) potassium uptake is regulated not only by the activity of the KdpD/KdpE two-component system (in turn influenced by PtsN). An additional controller with integrative behavior is predicted by the model structure. This suggests the presence of a novel physiological mechanism during regulation of potassium uptake with the KdpFABC transporter and may serve as a starting point for further investigations.

Introduction

Mathematical descriptions of complex interactions between the various components of a biochemical reaction network allow a quantitative understanding of network properties. With the advent of systems biology, which has led to the availability of high-dimensional datasets for metabolites, transcripts and proteins, a mathematical representation of such interactions becomes possible. Moreover, recent advances in experimental and theoretical methods now allow researchers to tightly integrate various types of data into the mathematical description of cellular processes. One of the key regulatory

1464–1801/15/0253–0178$39.50/0

E-Mail karger@karger.com
www.karger.com/mmb

A. Kremling
FG Systems Biotechnology, Technische Universität München
Boltzmannstrasse 15
DE–85748 Garching (Germany)
E-Mail a.kremling@lrz.tu-muenchen.de

devices in bacteria is the phosphotransferase system (PTS). This term describes a set of enzymes that transfer phosphate moieties derived from phosphoenolpyruvate (PEP) from one component to the other in a given order [Deutscher et al., 2006; Postma et al., 1993]. In general, two different types of PTS are found in bacteria: the sugar-PTS, responsible for the phosphorylation and uptake of carbohydrates into the cell, and the 'nitrogen-PTS' or PTS^{Ntr}, which fulfills exclusively regulatory functions [Pflüger-Grau and Goerke, 2010; Powell et al., 1995]. *Pseudomonas putida* possesses minimalistic PTS equipment with only one sugar-PTS responsible for fructose uptake (PTS^{Fru}) and the PTS^{Ntr}. Both PTS branches can communicate with each other by the exchange of phosphoryl groups [Pflüger and de Lorenzo, 2008].

Probably the best understood regulatory function of the PTS^{Ntr} is the control of the K^+ metabolism in *Escherichia coli* by direct interaction with both the TrkA subunit of the Trk transporter complex [Lee et al., 2007] and the KdpD sensor kinase of the two-component system (TCS) regulating the transcription of the *kdpFABC* genes [Lüttmann et al., 2009].

The KdpFABC P-type ATPase is a high-affinity K^+ transport system that ensures K^+ uptake when it becomes limiting and the cellular supply can no longer be served by the constitutive low-affinity K^+ transporting systems (Trk and Kup) [Altendorf et al., 1992; Ballal et al., 2007; Epstein, 2003; Schlosser et al., 1995]. The regulatory effect is brought about by the $EIIA^{Ntr}$ (PtsN) component by direct physical interaction of nonphosphorylated PtsN with the sensor kinase KdpD of the KdpD/KdpE TCS in *E. coli*. The binding of P-free PtsN stimulates the autophosphorylation activity of KdpD, resulting in increased transcription of *kdpFABC* [Lüttmann et al., 2009].

Recently, we carried out a genome-wide survey in *P. putida* to analyze the effects of the loss of PtsN on transcription. This revealed a strong impact on the transcript levels of the genes encoding the KdpFABC potassium transporter and the KdpD/KdpE TCS. Here, we present a theoretical approach based on linear system identification to analyze the influence of PtsN on *kdpFABC* transcription based on experimental data from *P. putida*. Therefore, we explored datasets with high temporal resolution of the wild-type strain and two PTS mutant strains grown with different K^+ concentrations. The data used included the optical density (OD), representing biomass growth, and luminescence (LUM), serving as an approximation for the expression of the *kdpFABC* genes. As little is known about the influence of biomass, the transcription and translation apparatus, and regulatory proteins on the expression of the *kdpFABC* genes, we started with a black box description. That is, a simple linear dynamical input/output description of the process, to set up a mathematical model. This model helps interpreting some of the complex processes taking place during regulatory events. Therefore it may serve as a starting point to further understand the molecular mechanism behind. Analysis of the dynamics uncovered expected and unexpected relations between the two variables measured, biomass and KdpFABC transporter production.

The Minimalistic PTS of P. putida

The Gram-negative soil bacterium *P. putida* is a perfect choice for studying the regulatory duties of the PTS^{Ntr} as it is equipped with the very low number of only five PTS proteins. Two proteins build the sugar-PTS (PTS^{Fru}) responsible for the uptake of fructose, and the other three are the components of the PTS^{Ntr}. PTS^{Fru} is encoded by *fruA* and *fruB*. The FruB protein combines the EI, HPr, and EIIA domain in one protein, and FruA builds the transporter consisting of the domains EIIB and EIIC, through which fructose is transported [Velazquez et al., 2007]. The alternative PTS^{Ntr} is formed by the proteins PtsP (EI^{Ntr}), PtsO (NPr), and PtsN ($EIIA^{Ntr}$) [Velazquez et al., 2007]. It is a multicomponent regulatory device that participates in controlling a variety of physiological processes in a posttranslational fashion. PtsP differs from the EI of the sugar-PTS by the presence of a GAF domain in its N-terminal part [Kundig et al., 1964; Pflüger-Grau and Görke, 2010; Reizer et al., 1996]. Recently, we published a mathematical model that describes the available data of the state of phosphorylation of PtsN in different environmental conditions and different strain variants [Kremling et al., 2012]. In *P. putida* the PTS^{Ntr} is quite well studied and several features are already known. In summary, it was shown that the phosphorylated form of PtsN is present at all growth stages and that it accumulates in the stationary phase. Therefore, the nonphosphorylated PtsN appears to be associated with rapid growth. The complete lack of PtsN leads to changes in the metabolic fluxes of the central carbon metabolism, and PtsN decreases the activity of pyruvate dehydrogenase by direct protein interaction [Chavarria et al., 2012; Pflüger and de Lorenzo, 2007, 2008; Pflüger-Grau et al., 2011]. All these findings give rise to a complex regulatory device in which diverse physiological inputs are integrated and result in a specific degree of phosphorylation of the PtsN protein, which, in turn, is involved in controlling the activity of a variety of physiological and metabolic processes.

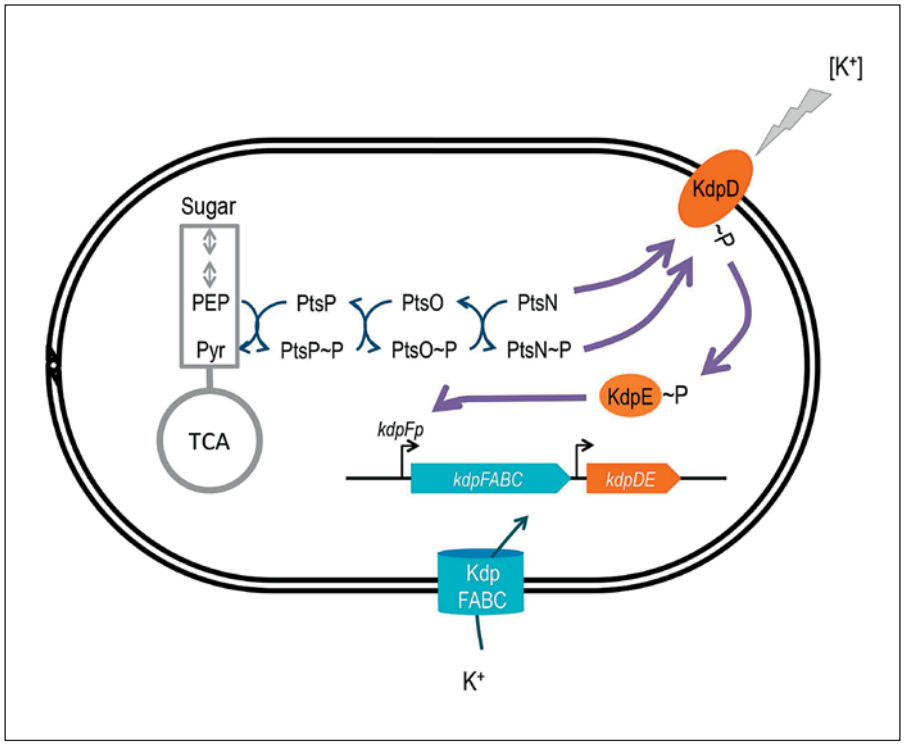

Fig. 1. Interplay of the Kdp potassium transport system and the PTS^{Ntr} in *P. putida*. The alternative PTS^{Ntr} is composed of three proteins: PtsP, PtsO, and PtsN, which transfer phosphate moieties derived from PEP from one enzyme to the other. Transcription of the KdpFABC potassium transporter encoding genes in *P. putida* is induced at low potassium concentrations (<1 mM extracellular K^+) by the activity of the KdpD/KdpE TCS. Direct interaction of PtsN with KdpD leads to altered *kdpFp* activities in that the presence of nonphosphorylated PtsN coincides with higher transcription rates, whereas the phosphorylated form of PtsN seems to have a negative effect on *kdpFABC* transcription.

The KdpFABC Potassium Transport Complex

Probably the best understood regulatory function of the PTS^{Ntr} is the control of K^+ metabolism in *E. coli* [Lee et al., 2007; Lüttmann et al., 2009]. Recently, we confirmed this interplay between PtsN and the KdpFABC transporter in *P. putida*, but the mechanism by which it is accomplished is different from what is known in *E. coli*. A genome-wide transcriptional survey to identify genes that are differentially expressed in the absence of PtsN in *P. putida* revealed that transcription of the entire *kdpFABC* operon as well as the *kdpDE* operon is strongly induced when PtsN is missing. The chromosomal organization of the *kdpFABC* and *kdpDE* genes in two operons adjacent to each other resembles the situation in *E. coli*, in which the KdpFABC P-type ATPase is well studied [Altendorf et al., 1992; Ballal et al., 2007]. It is a high-affinity K^+ transport system that ensures K^+ uptake under limiting conditions [Altendorf et al., 1992; Ballal et al., 2007; Epstein, 2003; Schlosser et al., 1995]. The KdpFABC K^+ transport complex is composed of four subunits: KdpA, the K^+ translocating channel; KdpB, which drives the K^+ translocation, and KdpF and KdpC, both involved in the assembly and stabilization of the transport complex [Buurman et al., 1995; Gassel et al., 1998, 1999; Haupt et al., 2005]. The KdpD/KdpE TCS controls transcription of *kdpFABC* [Polarek et al., 1992]. KdpD, the membrane-bound histidine kinase, autophosphorylates upon stimulus perception and subsequently hands over the phosphoryl group to the response regulator KdpE, which in turn binds to a specific site directly upstream of the *kdpFABC* promoter *(kdpFp)* [Laermann et al., 2013; Narayanan et al., 2012]. This strongly induces *kdpFABC* transcription [Ballal et al., 2007]. KdpD itself can act as a kinase as well as phosphatase, dephosphorylating KdpE in the absence of the stimulus [Jung et al., 1997], thereby shutting down transcription from *kdpFp*. The organization of the two operons *kdpFABC* and *kdpDE* adjacent to each other allows autoamplification of *kdpDE* transcription by the TCS [Polarek et al., 1992]. As already mentioned, in *P. putida* as well as in *E. coli* the activity of the KdpD/KdpE TCS is further regulated by direct binding of the PtsN protein, but in a different fashion. Whereas in *E. coli* only the nonphosphorylated form of PtsN interacts with KdpD, increasing the kinase activity and thereby stimulating transcription of the *kdpFABC* genes, in *P. putida* the mechanism is more complex in that both forms actively bind the KdpD sensor kinase, which results in opposite effects on the performance of *kdpFp*. Figure 1 illustrates the interplay between the PTS and the KdpD/KdpE TCS.

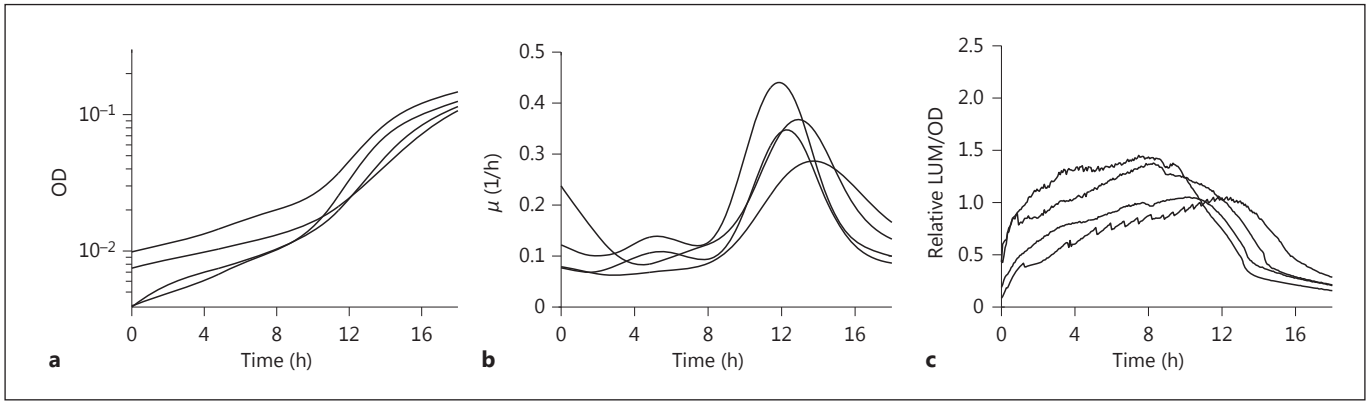

Fig. 2. Splined OD (**a**), specific growth rate μ (**b**) and the ratio LUM/OD (**c**) for a standard experiment with a potassium concentration of 10.12 mM. Four biological replicates are shown. The relative LUM/OD values are obtained by dividing the LUM data by the OD, and the normalization by the maximum of the LUM/OD values for an external potassium concentration of 0.22 mM.

Results

Time-Course Data

The experimental data used in this study came from measurements of OD and LUM of *P. putida* cells grown in minimal medium with varying K^+ concentrations (end concentrations: 0.22, 0.27, 0.32, 0.71, 1.21, 2.2, 5.17, 10.12, and 22 mM). LUM represents the amount of KdpFABC complexes produced as confirmed by Western blots and the OD serves as an approximation of the cell number. To determine the specific growth rate μ, the OD curve was smoothed to avoid fluctuations during calculation of the derivative $\Delta OD/\Delta t$. This smoothing was done by the *spaps* function of Matlab, which is based on an approach published by Reinsch [1967] to calculate smoothing splines. The maxima of the LUM/OD values of all strains and potassium concentrations, representing the maximal amount of KdpFABC complexes produced, are given in table 1.

For parameter estimation the time-course values were normalized by the maximum average LUM/OD value at a K^+ concentration of 0.22 mM. In figure 2, a representative dataset of the *ΔptsN* strain consisting of OD, specific growth rate μ and the LUM/OD ratio as an approximation of the intracellular concentration of the KdpFABC complexes is shown. The potassium concentration provided at the beginning of the experiment was 10.12 mM.

Interestingly, our data reveal that the growth rate is not constant during the exponential growth phase but changes from the very beginning of the experiment until the end. We assume that this behavior became visible, as we have collected 272 data points that were all used to calculate the growth rate, which results in highly resolved data for the specific growth rate μ. This allows us a more precise parameter identification, as the specific growth rate is known for each single time point.

Table 1. Unscaled maximal average values of LUM/OD for strains and external potassium concentrations

K^+/strain, mM	*ΔptsN*	*ptsNHA*	Wild-type
0.22	$7.60 \cdot 10^6$	$7.23 \cdot 10^6$	$5.91 \cdot 10^6$
0.27	$9.61 \cdot 10^6$	$8.89 \cdot 10^6$	$3.90 \cdot 10^6$
0.32	$8.71 \cdot 10^6$	$8.87 \cdot 10^6$	$3.79 \cdot 10^6$
0.71	$10.75 \cdot 10^6$	$10.66 \cdot 10^6$	$2.15 \cdot 10^6$
1.21	$11.62 \cdot 10^6$	$11.99 \cdot 10^6$	$9.35 \cdot 10^5$
2.20	$13.40 \cdot 10^6$	$11.53 \cdot 10^6$	$1.49 \cdot 10^5$
5.17	$12.13 \cdot 10^6$	$8.50 \cdot 10^6$	$3.44 \cdot 10^4$
10.12	$8.85 \cdot 10^6$	$4.87 \cdot 10^6$	$3.41 \cdot 10^4$
22	$5.10 \cdot 10^6$	$1.14 \cdot 10^6$	$3.21 \cdot 10^4$

Generalized Modeling Approach

Several approaches exist to deriving a mathematical model from experimental data (fig. 3). In recent years, the development of detailed mechanistic models has become quite common as more and more quantitative data of proteins and metabolites have become available. These mechanistic models are generally set up based on information derived from the literature and – in most cases – result in time-resolved simulation studies, which allow us the comparison of model outputs with measured data (fig. 3a). However, for the development of detailed mech-

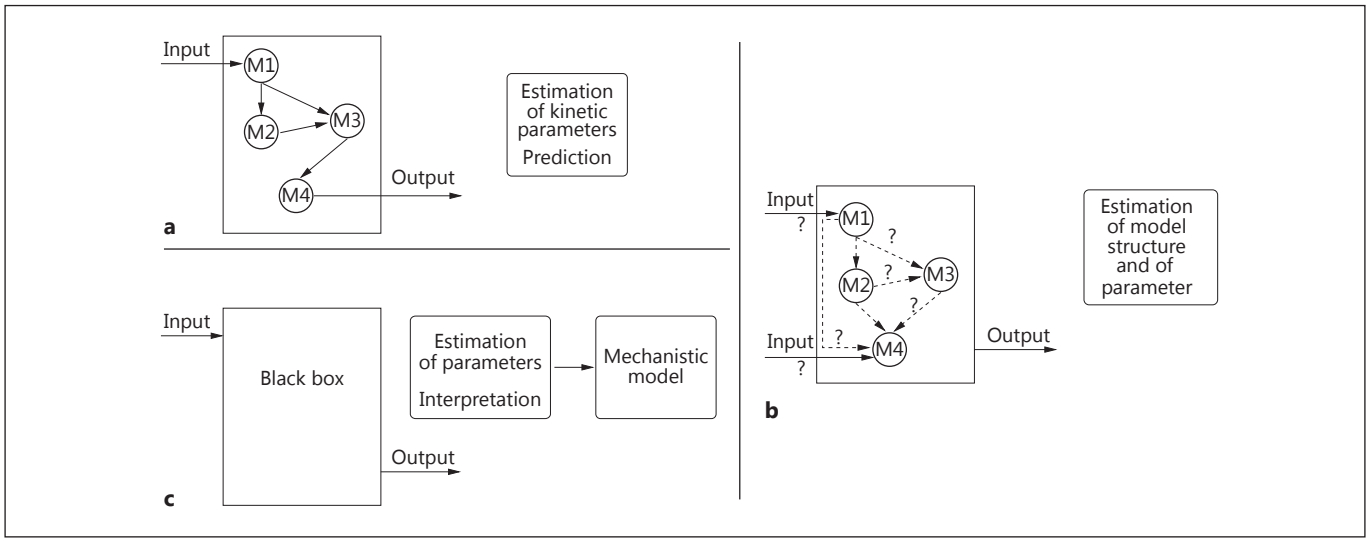

Fig. 3. Three model setup approaches. **a** If enough knowledge is available, a mechanistic model can be set up, parameters can be estimated, and the model can be used for prediction. **b** Ensemble modeling: model structure and kinetic parameters are determined from experimental data. **c** If not enough knowledge is available, an intermediate step is necessary to generate a first model from the data (generalized model) that serves as a basis for further model development.

anistic models it is necessary to have profound hypotheses on the involved partners and ways of interaction that can be translated into mathematical model equations. If the information on the network structure was uncertain or even unknown, an alternative approach that can be chosen to generate a mathematical model is ensemble modeling [Kuepfer et al., 2007]. This approach allows us to infer the model structure together with the kinetic parameters (the question marks in fig. 3b point to the uncertainty in the network structure). The main disadvantage of this approach is that measured data for all components in the network is required to develop a mathematical model.

A third approach that can be chosen when information is very limited is generalized modeling. This approach was chosen here as experimental data were available only for the OD and one intracellular component, the KdpFABC complex. No information on possible interactions between other intracellular components was accessible. In such a generalized modeling approach the system under investigation is considered as a black box (fig. 3c) and in a first step only the input/output behavior is described with a special type of equation. These equations are chosen in a way that they are as simple as possible but still able to describe the data with high accuracy. Thus, the advantage of the generalized modeling approach is that no a priori information on the network structure is necessary and parameters for the equations can be estimated using standard software tools. The biggest challenge of this approach is finding a meaningful biological interpretation of the equations.

For this work, experimental data representing the growth and intracellular KdpFABC complex concentration of three *P. putida* strains (wild-type, *ΔptsN* mutant and *ptsNHA* strain) grown at different potassium conditions were available. To set up a generalized model, we first divided the system under consideration into two submodules: the Kdp module, which describes the synthesis of the KdpFABC transporter and the PTS module representing the components of the PTS^{Ntr} (fig. 4). Additionally, a reference strain has to be chosen, which in this case was the *ΔptsN* mutant, as we expected that in this strain both modules exist separated from each other (reference situation) as no regulatory input from the PTS^{Ntr} on the Kdp module is present. The interconnection between the PTS module and the Kdp module by PtsN as present in the other two strains is represented by two different intervention strategies: strategy 1 involves distortion of the Kdp module only by P-free PtsN (data from the *ptsNHA* strain), whereas strategy 2 reflects the influence of both forms of PtsN (wild-type situation).

As can be seen in figure 4, two system inputs are considered: the growth rate (which influences both modules) and the external potassium concentration (which influ-

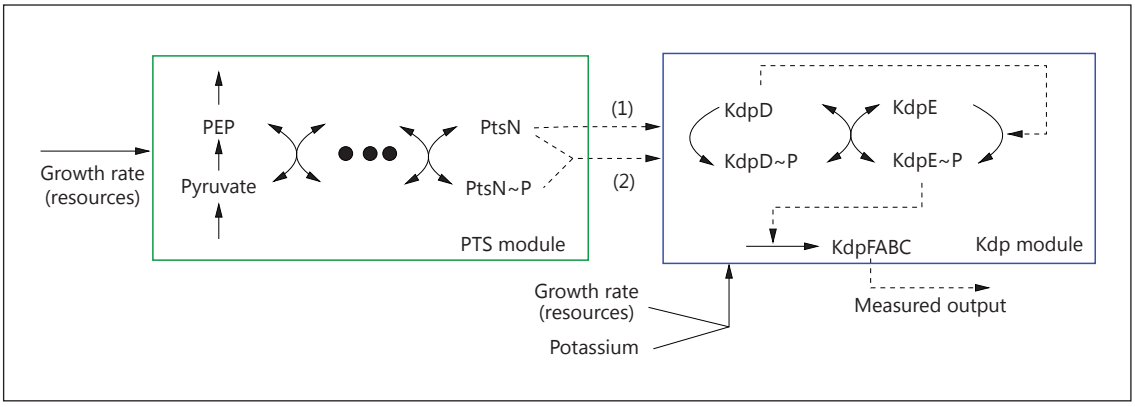

Fig. 4. Dissection of the system into two modules: PTS (green box) and KdpFABC transporter synthesis (blue box). Labels (1) and (2) indicate intervention strategies to disturb the system of the reference situation (*ΔptsN* mutant).

ences only the Kdp module). Time-resolved data for the growth rate was determined as described in Methods. The external potassium concentration at the beginning of the experiment is transformed into dynamic data by converting it into a step function, scaling the values between 0 and 1, i.e. the step size is taken as 1 for the highest potassium concentration of 22 mM and as 0.0091 for the lowest concentration of 0.22 mM.

Two different possibilities can be chosen as system output: the *kpdF* promoter activity or the concentration of the KdpFABC protein complex. Here, we decided to focus on the KdpFABC protein concentration as an output. This allows us to consider several processes, which can be divided roughly into 'positive' terms, reflecting processes that increase the concentration of the protein, like transcription and translation, and 'negative' terms, describing events that decrease the concentration of the component, like degradation, proteolysis or dilution. Dilution by growth is an often overlooked process that plays an important role when the temporal dynamics of a component are considered. It describes the alteration of the concentration of a component in the cell during cell division if no net synthesis of this component is present. Taking into account that directly before cell division the cell mass has doubled, the concentration (number of molecules per gram of dry weight) of the component has halved as the number of molecules has not changed.

An alternative choice for the output of the system is to focus on *kpdF* promoter activity. However, this would limit us to describing only the regulation of protein synthesis, including transcription and translation, and neglecting regulation by negative terms. In order to find a mathematical description for the experimental data at hand, we performed system identification, which is outlined in detail in Methods.

Parameter Estimation

ΔptsN Strain

The final model for the reference strain *ΔptsN* is given in state-space representation as follows (vector $\underline{x}$ has four components and vector $\underline{u}$ two components):

$$\dot{\underline{x}} = \begin{bmatrix} a_{11} & a_{12} & 0 & 0 \\ a_{21} & 0 & 0 & 0 \\ 0 & 0 & a_{33} & a^*_{43} \\ 0 & 0 & a^*_{43} & 0 \end{bmatrix} \underline{x} + \begin{bmatrix} b^*_{11} & 0 \\ 0 & 0 \\ 0 & b^*_{32} \\ 0 & 0 \end{bmatrix} \underline{u}$$

$$y = \begin{bmatrix} c_1 & 0 & c_3 & c_4 \end{bmatrix} \underline{x}. \qquad (1)$$

A clear block structure can be seen in the systems matrix which reflects the separation of the two inputs (growth rate u_1 and potassium concentration u_2). States x_1 and x_2 can be assigned to input u_1 while states x_3 and x_4 are assigned to input u_2. Both blocks are only connected by the output vector $\underline{c}$ and not in the systems matrix.

For parameter identification we chose the data obtained at one potassium concentration (here 1.21 mM) to fit the model structure and parameters (see Methods). Subsequently, data of the other potassium concentrations were fitted to the same model structure (parameter analysis was supported by the PottersWheel toolbox [Maiwald and Timmer, 2008] of Matlab). It turned out that

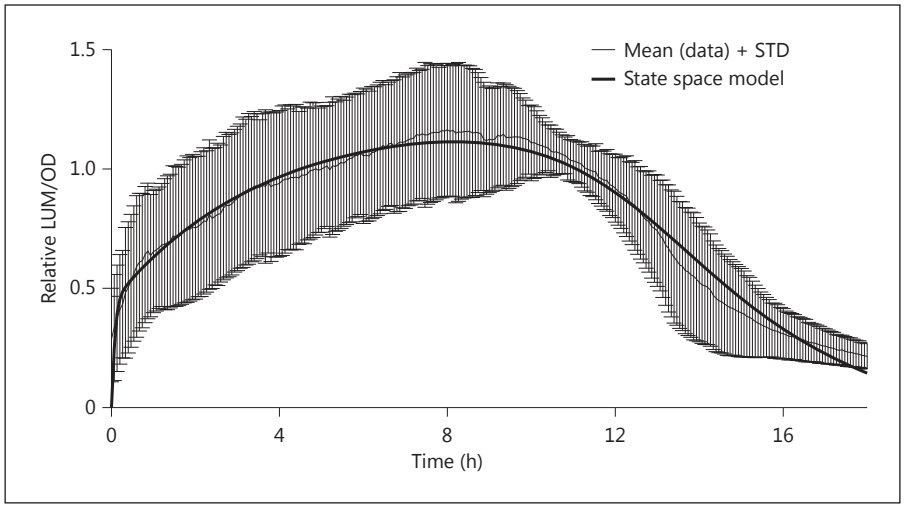

Fig. 5. Mean of the experimental data (LUM/OD) including error bars for a potassium concentration of 10.12 mM (gray region) and time course of the simulation after parameter estimation (solid black line).

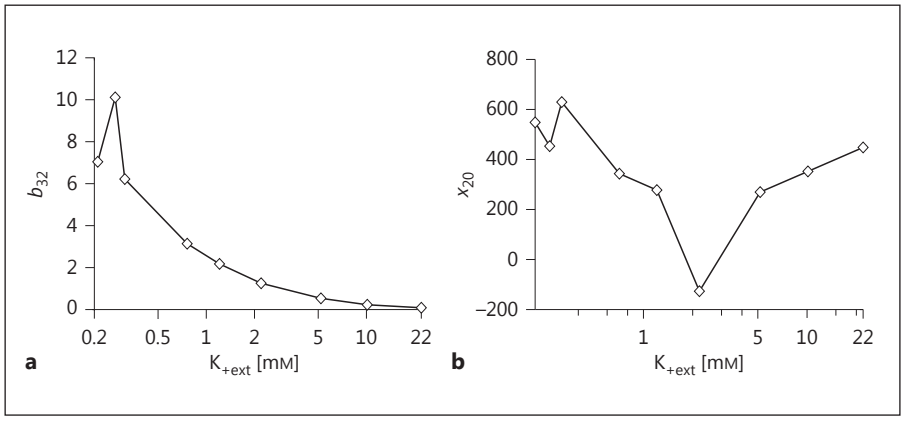

Fig. 6. a Parameter b_{32} is plotted over the external potassium concentrations for the *ΔptsN* model. **b** Estimated initial values x_{20} of the second state variable are plotted for different external potassium concentrations (fits were performed with one dataset, estimated initial values and a 'tfest' model structure).

some, but not all, parameters were strongly dependent on the input values. These input-dependent parameters (a_{34}, a_{43}, b_{11}, b_{32}) are highlighted by an * in equation 1. Figure 5 shows the quality of the parameter fit exemplarily for an external potassium concentration of 10.12 mM. The figure displays the mean of the experimental data with error bars based on four experiments (grey lines) and the model output (solid black line).

An example of a parameter that strongly depends on the input is parameter b_{32} (see the equation above). In figure 6a, the changes of b_{32} with varying potassium concentrations are shown. This parameter reflects the influence of input u_2 (potassium concentration) to the Kdp module. It is expected that this influence decreases at higher K^+ concentrations, which is confirmed by the decrease of parameter b_{32}. For comparison, in figure 6b, the result of a different parameter estimation which was based on initial values as parameters (see Methods) is shown. Here, for the initial value x_{20} no clear trend can be seen.

ptsNHA Strain

After having established a model for the reference strain with convincing accuracy and persuasive interpretability, the model structure was adjusted to fit the data of the *ptsNHA* strain (with the same number of state variables). Searching for a minimal parameter set to simulate the data of the potassium concentrations of 0.22, 1.21 and 10.12 mM revealed that it was necessary to introduce two more parameters, a_{24} and a_{42}. These new parameters represent connections between the state variables x_2 and x_4. Thereby, both submodules are now connected in a dynamic way and not only via the summation of the state variables in the output y. Thus, the dynamics of the first input (OD) now also influence the dynamics of the Kdp module (TCS and protein synthesis). This makes sense as in the *ptsNHA* strain a variant of the PtsN protein is present, which is supposed to influence KdpFABC transporter synthesis. The model for the *ptsNHA* strain is given in state space representation as follows:

$$\dot{\underline{x}} = \begin{bmatrix} a_{11} & a_{12} & 0 & 0 \\ a_{21} & 0 & 0 & a_{24} \\ 0 & 0 & a_{33}^* & a_{34}^* \\ 0 & a_{42} & a_{43}^* & 0 \end{bmatrix} \underline{x} + \begin{bmatrix} b_{11}^* & 0 \\ 0 & 0 \\ 0 & b_{32}^* \\ 0 & 0 \end{bmatrix} \underline{u}$$

$$y = \begin{bmatrix} c_1 & 0 & c_3 & c_4 \end{bmatrix} \underline{x}. \quad (2)$$

The model parameters for all 9 external potassium concentrations were determined. Thereby, it turned out that the newly introduced parameters a_{24} and a_{42} are constant over all potassium concentrations, whereas parameter a_{33} became potassium dependent and is therefore also highlighted with an * in equation 2.

Wild-Type Strain

Finally, the model for the wild-type strain was developed. We searched for a minimal parameter set to simulate the data for the potassium concentrations of 0.22, 1.21 and 10.12 mM. As was the case with the *ptsNHA* strain, the model for the wild-type strain also demanded the introduction of parameter a_{42}, whereas parameter a_{24} was no longer necessary to describe the experimental data. Parameter c_2* is now different from zero and potassium dependent, which leads to an influence of state variable x_2 at low external potassium concentrations on the system. Furthermore, a potassium dependency was introduced in c_1*, which resulted in similar quantitative levels of x_1, x_3 and x_4. Additionally, the whole system is damped compared to the two other strains, that is, that at higher potassium concentrations a lower response is observed. In order to make the parameter dependencies comparable, we introduced a factor c^*_{corr} that modifies all values of the $\underline{c}$ vector. The model structure for the wild-type is shown in state-space representation as follows (parameters varying over the external potassium concentration are highlighted using *):

$$\dot{\underline{x}} = \begin{bmatrix} a_{11} & a_{12} & 0 & 0 \\ a_{21} & 0 & 0 & 0 \\ 0 & 0 & a_{33} & a_{34} \\ 0 & a_{42} & a_{43} & 0 \end{bmatrix} \underline{x} + \begin{bmatrix} b_{11}^* & 0 \\ 0 & 0 \\ 0 & b_{32}^* \\ 0 & 0 \end{bmatrix} \underline{u}$$

$$y = c^*_{corr} \begin{bmatrix} c_1^* & c_2^* & c_3 & c_4 \end{bmatrix} \underline{x}. \quad (3)$$

The values of equation 4 (Methods) which serve to quantify the quality of parameter identification for the three strains and all external potassium concentrations are summarized in table 2. The values range between 46 and 85%.

Table 2. Parameter estimation: values for different strains and potassium concentrations according to equation 2

Concentration, mM	*ΔptsN*, %	*ptsNHA*, %	Wild-type, %
0.22	46.72	65.60	71.26
0.27	64.70	68.42	83.29
0.32	66.89	72.01	77.02
0.71	74.89	77.36	81.77
1.21	84.56	79.64	79.04
2.20	84.99	74.79	76.22
5.17	85.53	80.11	73.34
10.12	83.83	63.83	71.05
22.00	72.84	62.70	47.32

Comparison of Model Structures

The black box approach reveals dynamic connections between state variables, systems inputs and the output. For each strain variant considered here, the model structure had to be slightly refined in order to describe the experimental data. These modifications can be explained by taking into account the differences in the biochemical network structure of the reference strain and the other strains. The most prominent changes were the introduction of the connection between the PTS module and the Kdp module in the *ptsNHA* strain as well as in the wild-type strain. In these strains the PtsN protein is now present and therefore able to exert its regulatory functions on the Kdp module (fig. 4). Due to these connections it is expected that input 1, the OD, has a more direct influence on the second module in the *ptsNHA* strain and in the wild-type. The OD reflects the metabolic activity of carbon metabolism and is therefore directly related to the PTS.

Before comparing the different models in detail, we analyzed the dependence of the parameters on the external potassium concentration (fig. 7). As can be seen, only some kinetic parameters depend strongly on the potassium concentration, whereas others show a constant value.

In the next step we compared the model structures which were obtained from system identification. The interpretation of the simulation results is focused on the time-course simulation of the state variables x_1–x_4 of the three model variants. As an example we discuss here the results for each strain of an external potassium concentration of 0.27 mM.

ΔptsN Strain

Figure 8a shows the model structure for the reference strain *(ΔptsN)*. Parameters that are potassium dependent are highlighted within boxes. In the lower part of the figure, time courses of states x_1–x_4 are displayed.

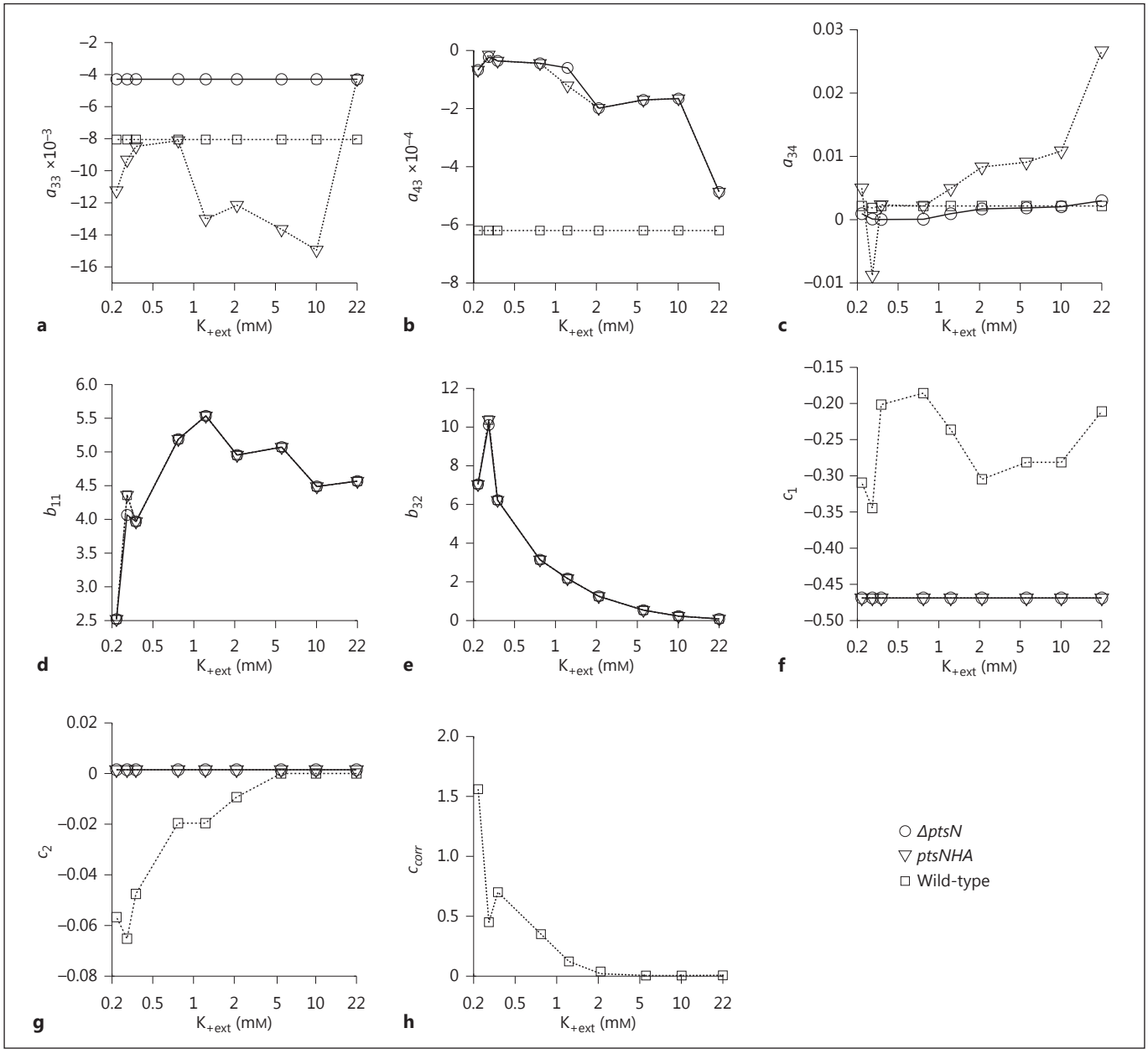

Fig. 7. Parameter dependencies on external potassium concentrations for all strain variants. **a** Parameter a_{33} shows different values for each strain but varies only for the *ptsNHA* strain with the external potassium concentration. **b** Parameter a_{43} shows the same pattern for *ΔptsN* and *ptsNHA*, but is constant for the wild-type. **c** Parameter a_{34} only varies for the wild-type strain. **d**, **e** Parameters b_{11} and b_{32} show a behavior in the opposite direction for all strains. **f–h** Parameters c_1, c_2 and c_{corr} vary just for the wild-type strain and have the same constant value for the *ΔptsN* and *ptsNHA* strains. Potassium concentrations are plotted on logarithmic scales to the highlight variations at small potassium concentrations.

As will be explained in detail in the following, the central message of this model structure is that in the *ΔptsN* strain the KdpFABC level (output) is influenced independently by three factors: the first is dilution by growth, the second is a fast response of the TCS to a potassium down shock, and the third is an integrative regulatory behavior. This integrative regulator steadily increases its signal when the shock cannot be overcome by intracellular processes.

As can be seen from the time-course data, only x_1 from the PTS module (green box) contributes to the system

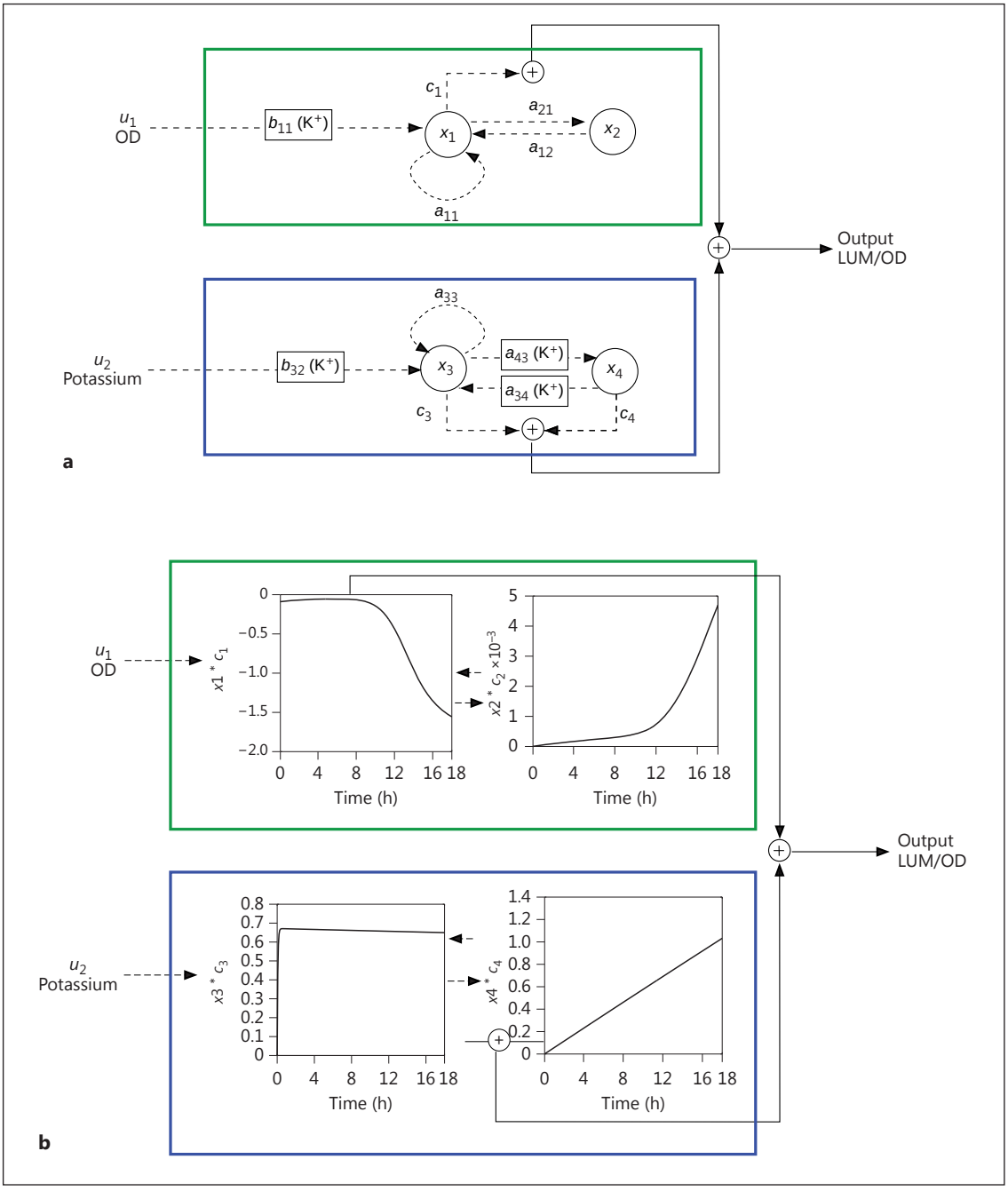

Fig. 8. a Model structure for the *ΔptsN* strain (reference strain); parameters varying over potassium are displayed in black boxes. **b** The time course of the internal state variables. The model was simulated with input data for an external potassium concentration of 0.27 mM.

output, as the values of x_2 are very small. Dynamics of x_1 together with x_2 generate a negative influence on the system output, as x_1 is always negative. The behavior of x_1 together with x_2 can be interpreted as the dilution term, a standard term in mass balance equations for intracellular metabolites. Dilution by growth takes into account the distribution of molecules to the daughter cells during cell division and is an important entity in the case that no flux of synthesis exists. Therefore, cells are able to reduce the number of molecules per cell just by dividing. Since in the

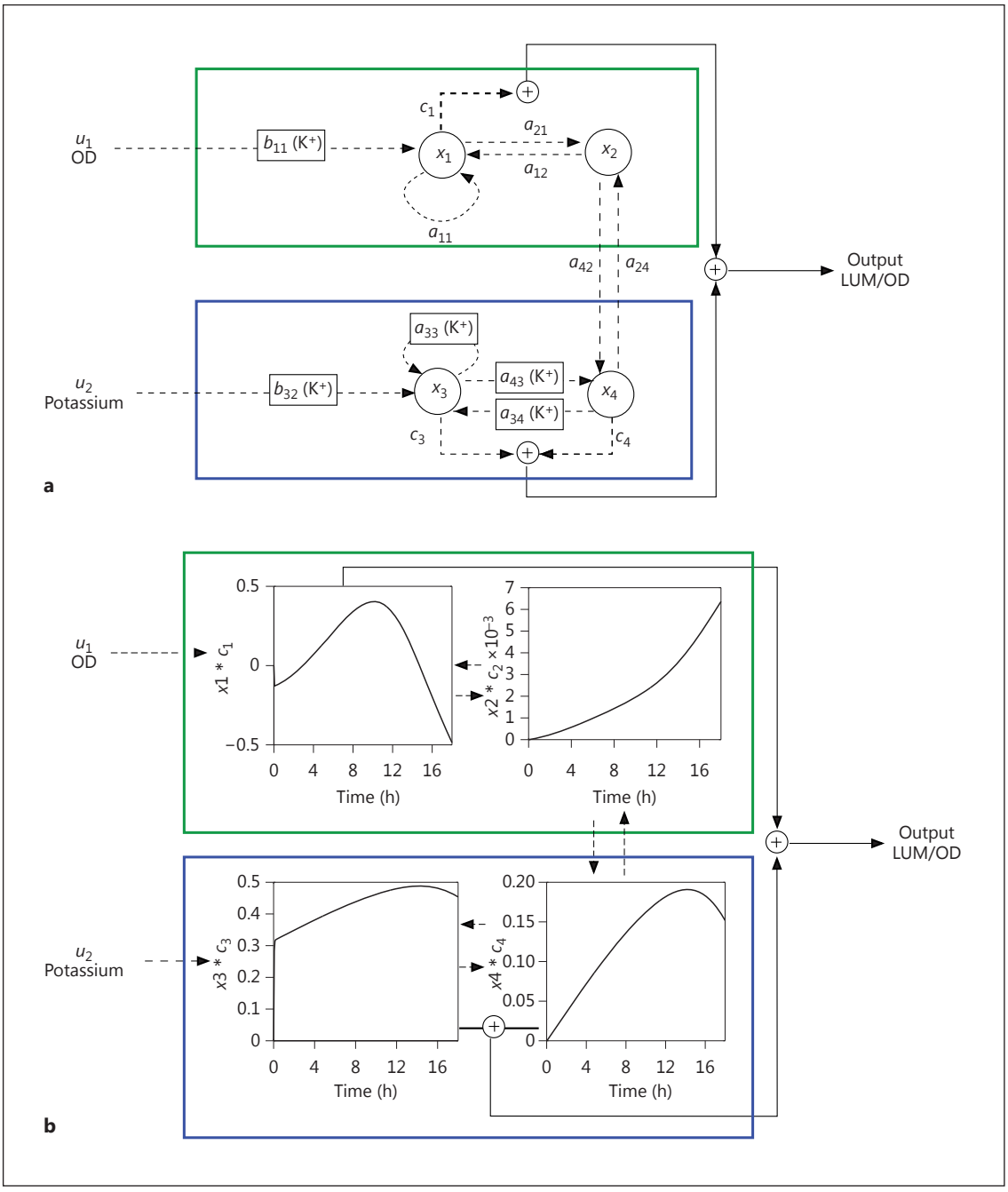

Fig. 9. a Model structure for the *ptsNHA* strain; parameters varying with the external potassium concentration are surrounded by boxes. **b** The time course of internal state variables. The model was simulated with input data for an external potassium concentration of 0.27 mM.

reference strain neither module is connected via PtsN, the influence of the growth rate is limited to the dilution effect. As can be seen in the figure, two parameters, b_{11} and b_{32}, connect the respective input u_1 and u_2 to the system variables, both of which depend on the potassium concentration (fig. 7d, e). While parameter b_{11} shows an increasing trend, parameter b_{32} shows a trend in the opposite direction. This observation reflects that, for higher extracellular potassium concentrations, the influence of potassium is reduced, while the OD becomes more prominent.

Analysis of the time-course data for x_3 and x_4 revealed that the system's response x_3 increases strongly directly after the start of the experiment and persists on a high level. In contrast, state variable x_4 increases steadily. State variable x_3 can be interpreted as a fast response of the system after a potassium down shift. Therefore, it might represent the dynamics of the TCS and the synthesis of the mRNA of the output protein. As signal x_4 is increasing over the whole time period, it could serve as a controller with integrative behavior. When cells are grown at low extracellular potassium concentrations, it is expected that the internal potassium pool will be completely depleted. Therefore, the cellular machinery has to be activated in order to compensate for the lack of potassium. However, as the external potassium concentration is very low, the cell's needs cannot be served by the activity of the KdpFABC transporter. As a consequence, an integral controller becomes active. This was already observed for bacterial chemotaxis where adaptation precision could be explained using a mathematical model [Alon et al., 1999]. If cells are grown at higher extracellular potassium concentrations, the system is able to adapt, as more potassium can be taken up and the time course of x_4 reaches a constant value after 12 h (data not shown).

ptsNHA Strain

The model structure of the *ptsNHA* strain is shown in figure 9a. The parameters that depend on the external potassium concentration are again marked with black boxes. In the lower part of the figure, the time courses of states x_1–x_4 are depicted.

The central message of the model structure of the *ptsNHA* strain is that here the KdpFABC level (output) is influenced by four effects. As in the *ΔptsN* strain model, dilution by growth, a fast reaction of the TCS and the integrative regulator play a role. Furthermore, the new connection between two state variables (by parameters a_{42} and a_{24}) now results in a positive, growth-dependent influence on the Kdp module. We propose that this influence is a consequence of the presence of the unphosphorylated PtsN protein. This results in increased KdpFABC production in a growth-dependent manner. In the following these statements will be explained in more detail.

The construction of the model for the *ptsNHA* strain, while preserving the structure of the model of the *ΔptsN* strain, required the inclusion of two new connections, a_{42} and a_{24}, between state variables x_2 and x_4. While the time course of x_3 and x_4 are qualitatively similar in both model variants for the first 12 h, state variable x_1 now shows positive values. We interpret this positive signal as the influence of the PTS^{Ntr} (included in the first module) on the potassium uptake system KdpFABC. As the PTS module is basically represented by x_1, as x_2 is again close to zero, it reflects both a positive activator of the KdpFABC synthesis and dilution by growth as already described for the reference strain. Again, x_3 reacts with a sharp increase directly after the potassium down shock and a slow but steady increase afterwards. However, it does not reach the same steady state as in the *ΔptsN* strain model. State variable x_4 is again interpreted as a controller with integrative behavior, but for the *ptsNHA* strain the signal is not as strong as for the reference strain. As already described for *E. coli*, PtsN influences the activity of the KdpD/KdpE TCS by direct interaction with the sensor kinase KdpD, which in turn senses the potassium availability [Lüttmann et al., 2009]. In comparison to the *ΔptsN* strain model where the PTS and the Kdp modules existed separated from each other, in the model for the *ptsNHA* strain the influence of the PTS module on the output became more prominent. This reflects the influence of the growth rate and the PTS^{Ntr} on the synthesis of the KdpFABC transport complex.

Wild-Type Strain

The final model structure of the wild-type strain is shown in figure 10a. Again, the parameters that change with variations in the external potassium concentration are marked with black boxes. The lower part of the figure displays the time courses of states x_1–x_4.

Analyzing the model structure and parameter dependencies in the wild-type, it turned out that the KdpFABC level is regulated in a different way as compared to the other two strains. Dilution by growth, a fast reaction by the TCS and the integrative regulator exist as in the *ΔptsN* and *ptsNHA* strains. However, a negative influence in late growth stages can now be observed that is derived from the phosphorylated PtsN molecule. The whole system is damped, that is, the expression rate is lower, and is deactivated at external potassium concentrations higher than 1 mM due to the introduction of the phosphorylated PtsN protein.

A closer inspection of the model structure revealed that the model for the wild-type strain is characterized by major alterations. State variable x_2 becomes relevant for the output at low potassium concentrations and the complex building parameter a_{24} is no longer necessary. Furthermore, in contrast to the other strains, output parameter c now partly depends on the external potassium concentration (see fig. 7h). As in the reference strain *(ΔptsN)*,

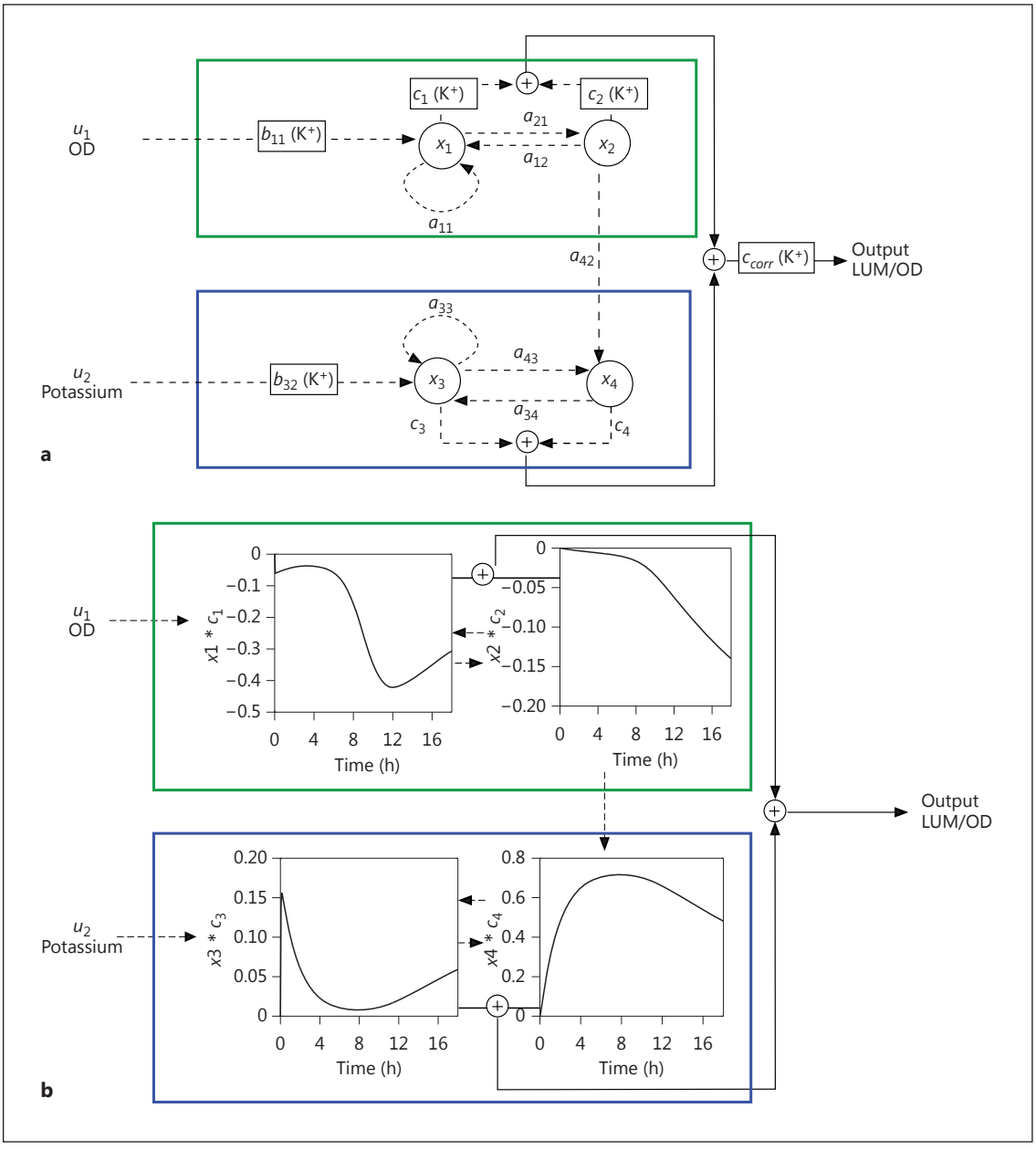

Fig. 10. a Model structure for the wild type strain; parameters varying with the external potassium concentration are highlighted by boxes. **b** The time course of internal state variables. The model was simulated with input data for an external potassium concentration of 0.27 mM.

state variables x_1 negatively contributes to the output and represent only dilution by growth. The positive influence seen in the *ptsNHA* strain is not observed in the wild-type. This can be explained by the fact that in the wild-type PtsN is present in both forms, phosphorylated and non-phosphorylated, whereas in the *ptsNHA* strain it is locked in the P-free form.

The time course of state variable x_3 shows the biggest difference in comparison to the other two strains. After a fast increase a slow decrease is observed. This can be interpreted as a fast adaptation to the new environmental conditions. A reduction of the TCS activity results due to additional potassium uptake by the KdpFABC transport complex. The time course for all external potassium con-

centrations is very similar, but differs in the output vector *c*. As can be seen in figure 7, values for parameter c_{corr}, which is a weight for the overall output of the states, decreases with increasing potassium concentration. This reflects a superimposed control scheme balancing the dynamics influenced by the growth rate and the external potassium concentration which is valid only in the wild-type strain.

In summary, all experimental data for the three strain variants could be described using a model that is composed of four state variables. State variables x_1 and x_2 could be assigned to input u_1 (growth rate, PTS module), while state variables x_3 and x_4 were assigned to input u_2 (external potassium concentration, Kdp module).

Interpretation and Biological Meaning

The PTS is one of the most prominent signal transduction units in bacteria and quite well studied, especially in *E. coli* and *P. putida* [Deutscher et al., 2006]. It measures the flux through glycolysis and gluconeogenesis by mapping the ratio of intracellular PEP and pyruvate to the degree of phosphorylation of the PTS proteins [Deutscher et al., 2006; Kremling et al., 2007]. For the carbohydrate branch in *E. coli*, the degree of phosphorylation is linked to the activation of the global transcription factor Crp. The TF which positively and/or negatively influences more than 260 operons (for example, see database Ecocyc) and is the most important regulator for carbohydrate metabolism. Mathematical models for carbohydrate uptake and control are already available [Baldazzi et al., 2010; Bettenbrock et al., 2006; Kotte et al., 2010] and provide a quantitative approach for the understanding of the complex interaction scheme between metabolism, signaling and gene expression.

In contrast, the role of the PTS^{Ntr} is less well understood and mathematical models are scarce [Kremling et al., 2012]. From studies with *E. coli* an interrelation of the components of the PTS^{Ntr} with potassium metabolism was described. In this study, we analyzed the interaction of PtsN with the sensor kinase KdpD in *P. putida* by monitoring the effect of different extracellular potassium concentrations on the production of the KdpFABC potassium transport complex of the wild-type and two *pts* mutant strains. Potassium is a major cation and involved in the regulation of cell turgor and pH homeostasis. In the study at hand we focused on the interplay between the PTS^{Ntr} and the expression of the *kdpFABC* operon in *P. putida*. Based on time-course data for three strain variants in combination with nine different initial potassium concentrations, a broad range of conditions was covered.

In contrast to a recently published mathematical model, which describes gene expression dynamics for *E. coli* in the absence of potassium [Heermann et al., 2014], here only the time course for the KdpFABC protein was determined and measurements for other intracellular components like mRNA or intracellular potassium were not performed. Therefore, we chose a different modeling strategy: the system was considered as a black box and generalized models for each strain variant were identified. The criteria that were applied to choosing the final model were the quality of the parameter estimation (a quantitative measure) and the interpretation of the results in a physiologically meaningful way (a qualitative measure). Bearing in mind that the behavior of cellular systems is strongly nonlinear, the results of parameter estimation was satisfactory as the fit values were between 46 and 85%.

In our study the *ΔptsN* mutant was chosen as the reference strain, as the interaction of potassium metabolism with PTS^{Ntr} should be disabled in this strain due to the lack of the PtsN protein. The *ptsNHA* strain produces a variant of the PtsN protein that carries an amino acid exchange at the phosphorylation site from histidine to alanine, which results in a protein that is blocked in the non-phosphorylated form. In contrast, in the wild-type both forms of PtsN are present at the same time, although in varying ratios.

In the reference strain both modules act independently of each other, as there is no internal connection between the PTS^{Ntr} and KdpFABC protein synthesis because the PtsN protein is not produced in this strain. The time course of the KdpFABC protein could be described using a linear superposition of the output of both modules, reflecting the influence of dilution by growth and the influence of the external potassium concentration. While the dynamics of the first module could clearly be assigned to the dilution effect, the second module is more difficult to interpret. The simulation shows a typical behavior for signaling and mRNA synthesis, which consists of a rapid first response and a subsequent adaptation. This has also been described for the regulation of potassium homeostasis in *E. coli*, where signaling processes like TCSs and feedback control elements are known to play an important role [Heermann et al., 2014]. Interestingly, this was not sufficient to completely explain the measured data. It turned out that an additional element had to be incorporated which later on could be interpreted as an intracellular controller. At low potassium concentrations, cells

are not able to reach potassium homeostasis and, therefore, the state variable representing the intracellular controller increases over time, displaying the cell's increasing need for potassium. At higher potassium concentrations the state variable of the controller is constant over a longer time period. In this strain, in which no PtsN protein is present and therefore no additional influence on the KdpD sensor kinase is expected, a higher expression of *kdpFABC* is observed than in the wild-type, where both forms of PtsN are present. This indicates a strong inhibitory effect of either phosphorylated or the P-free PtsN on the activity of the *kdpFp* via KdpD.

In the *ptsNHA* strain only unphosphorylated PtsN is present and during model identification it became obvious that now an internal connection between the two modules had to be incorporated. In comparison to the reference strain, the dynamics obtained show striking differences: the output of the PTS module shows positive values and the Kdp module output has lower values. This indicates a stronger influence of the growth rate/PTS^{Ntr} on *kdpFABC* gene expression in the presence of P-free PtsN than in its absence (reference strain). In the wild-type strain, however, in which both forms of the PtsN protein are present, KdpFABC production is lower than in the other two strains. This effect is pronounced at higher potassium concentrations. We attributed the lower KdpFABC production to the presence of the phosphorylated form of PtsN, which seems to have a strong negative effect and to slow down gene expression at already low external potassium concentrations. The potassium dependency of the system is also reflected by the course of the output parameter c_{corr}, which enhances the output at low potassium concentrations and approaches zero at potassium concentrations around 2 mM.

Based on linear system identification, we were able to generate model variants which successfully describe high resolution time-course data for the potassium transporter KdpFABC. These models present a promising starting point for the development of mechanistic models for the interaction of the PTS^{Ntr} with the potassium subnetwork in *P. putida*. The absence of the PtsN protein leads to strong KdpFABC production even in the presence of high extracellular potassium concentrations. This should result in unnaturally high intracellular potassium concentrations, which could be an explanation for the reduced growth rate observed in this strain. It is tempting to speculate that PtsN is a potent regulator of the KdpD activity, especially at high extracellular potassium concentrations, downregulating the amount of KdpFABC complexes produced. As no downregulatory activity was observed in the *ptsNHA* strain, we attributed the repressive effect to the phosphorylated form of PtsN. In such a mechanistic model the interaction between the proteins KdpD, KdpE and PtsN will play a major role and we speculate that this 'three-component system' can integrate signals from carbohydrate metabolism (transferred by the phosphorylation state of PtsN) and potassium metabolism (sensed by KdpD). From bacterial two-hybrid experiments we have strong indications that the influence of PtsN on transcription of the *kdpFABC* operon is mediated through direct interaction between PtsN and KdpD [unpubl. data]. Together, these studies pave the way towards a detailed modeling of the influences of the PTS^{Ntr} on potassium homeostasis and, therefore, may lay the foundation for more thorough understanding of the interaction between carbohydrate and potassium metabolism.

Table 3. Strains used in this study

Strain	Description
P. putida KT2440	Wild-type
P. putida ΔptsN	Strain carrying a markerless deletion of the entire *ptsN* gene
P. putida ptsNHA	Strain producing a variant of the PtsN protein bearing an amino acid exchange in position 68 from His to Ala (which locks PtsN in a nonphosphorylated state)

Methods

Strain Construction

All *P. putida* strains used in this work are derived from *P. putida* KT2440 [Nelson et al., 2002]. *P. putida ΔptsN* was constructed using the method described by Martínez-García and de Lorenzo [2011]. *P. putida ptsNHA* was basically constructed as described in Pflüger-Grau et al. [2011], with the only difference being that *P. putida* KT2440 served as the recipient strain. In each case, the mutation was confirmed by sequencing the respective region. An overview of all strains used in this study is given in table 3. Plasmid pSEVA226_kdp, bearing a transcriptional fusion of the *kdpFABC* promoter region with the *luxCDABE* genes, was constructed by ligating a fragment spanning a sequence from 565 bp upstream of the start codon of *kdpF*, containing the predicted −10 and −35 box of the *kdpFABC* promoter *(kdpFp)* into the multiple cloning site of pSEVA226 [Silva-Rocha et al., 2013]. This allowed the measurement of activity of *kdpFp* by monitoring luminescence (LUM) and optical density (OD) of growing cells directly in the automated microplate reader Infinite M200 Pro (Tecan, Männedorf, Switzerland). The ratio of LUM/OD served as a good approximation for the concentration of the KdpFABC protein in the cell as confirmed by Western blotting with a specific antiserum against the KdpFABC complex.

Table 4. System identification overview: initial value setting, used datasets, and chosen inputs for the black box system identification

Dataset	one dataset				one dataset			
$Input_1$	OD							
$Input_2$	potassium				potassium			
Output	LUM/OD				LUM/OD			
Initials	estimated				estimated			
Tool	tfest	bj	arx	ssest	tfest	bj	arx	ssest
Dataset	nine datasets				nine datasets			
$Input_1$	OD							
$Input_2$	potassium				potassium			
Output	LUM/OD				LUM/OD			
Initials	zero				zero			
Tool	tfest	bj	arx	ssest	tfest	bj	arx	ssest

Data Generation

To determine the expression of the *kdpFABC* operon, cells carrying pSEVA226_kdp were directly grown in black 96-well plates with transparent bottoms and lids (Brand, Wertheim, Germany) in 200-µl potassium-free M9 medium with 0.2% citrate with varying potassium concentrations (0–22 mM). Wells were inoculated with 2 µl of an overnight culture of the respective strain grown with 22 mM of potassium, and the plates were incubated in the automated microplate reader Infinite M200 Pro (Tecan) at 30°C with orbital shaking before every measurement. The OD at 600 nm and LUM were measured at least every 4 min. Each value used in parameter estimation represents the mean of at least 4 independent experiments.

System Identification

System identification is a basic method in engineering sciences to find a mathematical description of a system. It is applied to determine the structure of the model and to analyze and estimate the parameters of the model. Therefore, the following steps are usually performed: (i) fixing a model structure, (ii) setting the order of the model (that means the number of state variables that are used to characterize the system) and (iii) parameter identification, including parameter analysis (which parameter can be estimated based on the experimental data) and parameter estimation itself.

Here, generalized models were used that describe the connection between inputs and outputs of a system. Various types of such models are described in the literature and implemented in the software package Matlab (www.mathworks.com). Models that are provided by the toolbox vary in the design of the model structure (Matlab functions 'tfest', 'bj', 'arx' and 'ssest' are used) and in the choice of the initial values for the state variables (initial values could be set at zero or can be regarded as additional parameters which must be estimated).

The use of the toolbox requires a special data format, which consists of input data, output data and a time vector. The input and output data can represent multiple experiments. We tried two different approaches to convert the time-course data into datasets: in the first a single dataset was created using all 9 potassium concentrations (with 4 biological replicates each), whereas in the second approach the data for each potassium concentration (with 4 biological replicates each) was considered individually. This generated 9 datasets, one for each potassium concentration. First we fitted the data from the reference strain *(ΔptsN)* to find a suitable model structure. The best model structure found served as the basis for the other two strains (*ptsNHA* and wild-type). Furthermore, we analyzed the difference between using either potassium as the single input or potassium and OD as combined inputs. Altogether, this resulted in 16 different combinations of datasets for system identification, which are summarized in table 2. The final result of the whole process of system identification is a set of differential equations with corresponding parameters.

The final result of system identification is described in detail in the Results section. Once a suitable system is identified, it is necessary to evaluate the outcome. Here, two criteria come into play. The first criterion is the quality of the fit of the model. The toolbox provides a quantitative measure that was used to scale the difference between the model simulation and the experimental data. The numbers can range between 0 and 100, with 100 representing a perfect fit:

$$fit = 100 \times \left(1 - \frac{\| Data - Model \|^2}{\| Data - mean\left(Model\right) \|^2}\right). \quad (4)$$

The second criterion is the interpretability of the model. This is crucial as it cannot be quantified but is based on the experience and intuition of the model developer. Interpretability in this context is defined as the ability of the user to assign a biological function/meaning to the proposed model structure. The interpretability of these structures depends greatly on the number of components and the number of connections between these components. For example, a serial connection of 20 components having 19 connections is easier to interpret than a spiderweb-like network of just 6 components and 24 connections. Another point which influences the interpretability is the potential dependence of the parameter values on the potassium concentration. As described above, here two alternatives for parameter identification were analyzed. The first approach tried to find a single set of parameters for all conditions, while the second one aimed to find a separate parameter set for each potassium concentration. After considering all the identification variants shown in table 4, the best model structure turned out to be the one based on 9 datasets, using two inputs, zero initial values and the 'tfest' function.

References

- Alon U, Surette MG, Barkai N, Leibler S: Robustness in bacterial chemotaxis. Nature 1999; 397:168–171.
- Altendorf K, Siebers A, Epstein W: The KDP ATPase of *Escherichia coli*. Ann NY Acad Sci 1992;671:228–243.
- Baldazzi V, Ropers D, Markowicz Y, Kahn D, Geiselmann J, de Jong H: The carbon assimilation network in *Escherichia coli* is densely connected and largely sign-determined by directions of metabolic fluxes. PLoS Comp Biol 2010;6:e1000812.
- Ballal A, Basu B, Apte SK: The Kdp-ATPase system and its regulation. J Biosci 2007;32:559–568.

Bettenbrock K, Fischer S, Kremling A, Jahreis K, Sauter T, Gilles ED: A quantitative approach to catabolite repression in *Escherichia coli*. J Biol Chem 2006;281:2578–2584.

Buurman ET, Kim KT, Epstein W: Genetic evidence for two sequentially occupied K^+ binding sites in the Kdp transport ATPase. J Biol Chem 1995;270:6678–6685.

Chavarria M, Kleijn RJ, Sauer U, Pflüger-Grau K, de Lorenzo V: Regulatory tasks of the phosphoenolpyruvate-phosphotransferase system of *Pseudomonas putida* in central carbon metabolism. mBio 2012;3:e00028-12.

Deutscher J, Francke C, Postma PW: How phosphotransferase system-related protein phosphorylation regulates carbohydrate metabolism in bacteria. Microbiol Mol Biol Rev 2006; 70:939–1031.

Epstein W: The roles and regulation of potassium in bacteria. Prog Nucleic Acid Res Mol Biol 2003;75:293–320.

Gassel M, Mollenkamp T, Puppe W, Altendorf K: The KdpF subunit is part of the K^+-translocating Kdp complex of *Escherichia coli* and is responsible for stabilization of the complex in vitro. J Biol Chem 1999;274:37901–37907.

Gassel M, Siebers A, Epstein W, Altendorf K: Assembly of the Kdp complex, the multi-subunit K^+-transport ATPase of *Escherichia coli*. Biochim Biophys Acta 1998;1415:77–84.

Haupt M, Bramkamp M, Coles M, Kessler H, Altendorf K: Prokaryotic Kdp-ATPase: recent insights into the structure and function of KdpB. J Mol Microbiol Biotechnol 2005;10: 120–131.

Heermann R, Zigann K, Gayer S, Rodriguez-Fernandez M, Banga JR, Kremling A, Jung K: Dynamics of an interactive network composed of a bacterial two-component system, a transporter and K^+ as mediator. PloS One 2014; 9:e89671.

Jung K, Tjaden B, Altendorf K: Purification, reconstitution, and characterization of KdpD, the turgor sensor of *Escherichia coli*. J Biol Chem 1997;272:10847–10852.

Kotte O, Zaugg J, Heinemann M: Bacterial adaptation through distributed sensing of metabolic fluxes. Mol Syst Biol 2010;6:355–355.

Kremling A, Bettenbrock K, Gilles ED: Analysis of global control of *Escherichia coli* carbohydrate uptake. BMC Syst Biol 2007;1:42.

Kremling A, Pflüger-Grau K, Chavarria M, Puchalka J, Martins dos Santos V, de Lorenzo V: Modeling and analysis of flux distributions in the two branches of the phosphotransferase system in *Pseudomonas putida*. BMC Syst Biol 2012;6:149.

Kuepfer L, Peter M, Sauer U, Stelling J: Ensemble modeling for analysis of cell signaling dynamics. Nat Biotechnol 2007;25:1001–1006.

Kundig W, Ghosh S, Roseman S: Phosphate bound to histidine in a protein as an intermediate in a novel phospho-transferase system. Proc Natl Acad Sci USA 1964;52:1067–1074.

Laermann V, Cudic E, Kipschull K, Zimmann P, Altendorf K: The sensor kinase KdpD of *Escherichia coli* senses external K^+. Mol Microbiol 2013;88:1194–1204.

Lee CR, Cho SH, Yoon MJ, Peterkofsky A, Seok YJ: *Escherichia coli* enzyme IIA^{Ntr} regulates the K^+ transporter TrkA. Proc Natl Acad Sci USA 2007;104:4124–4129.

Ljung L: System Identification: Theory for the User. Toronto, Pearson Education Canada, 1987.

Lüttmann D, Heermann R, Zimmer B, Hillmann A, Rampp IS, Jung K, Görke B: Stimulation of the potassium sensor KdpD kinase activity by interaction with the phosphotransferase protein IIA^{Ntr} in *Escherichia coli*. Mol Microbiol 2009;72:978–994.

Maiwald T, Timmer J: Dynamical modeling and multi-experiment fitting with PottersWheel. Bioinformatics 2008;24:2037–2043.

Martínez-García E, de Lorenzo V: Engineering multiple genomic deletions in Gram-negative bacteria: analysis of the multi-resistant antibiotic profile of *Pseudomonas putida* KT2440. Environ Microbiol 2011;13:2702–2716.

Narayanan A, Paul LN, Tomar S, Patil DN, Kumar P, Yernool DA: Structure-function studies of DNA binding domain of response regulator KdpE reveals equal affinity interactions at DNA half-sites. PLoS One 2012;7:e30102.

Nelson KE, Weinel C, Paulsen IT, Dodson RJ, Hilbert H, Martins dos Santos VA, Fouts DE, Gill SR, Pop M, Holmes M, Brinkac L, Beanan M, DeBoy RT, Daugherty S, Kolonay J, Madupu R, Nelson W, White O, Peterson J, Khouri H, Hance I, Chris Lee P, Holtzapple E, Scanlan D, Tran K, Moazzez A, Utterback T, Rizzo M, Lee K, Kosack D, Moestl D, Wedler H, Lauber J, Stjepandic D, Hoheisel J, Straetz M, Heim S, Kiewitz C, Eisen JA, Timmis KN, Dusterhoft A, Tummler B, Fraser CM: Complete genome sequence and comparative analysis of the metabolically versatile *Pseudomonas putida* KT2440. Environ Microbiol 2002;4:799–808.

Pflüger K, de Lorenzo V: Growth-dependent phosphorylation of the PtsN ($EIIA^{Ntr}$) protein of *Pseudomonas putida*. J Biol Chem 2007; 282:18206–18211.

Pflüger K, de Lorenzo V: Evidence of in vivo cross talk between the nitrogen-related and fructose-related branches of the carbohydrate phosphotransferase system of *Pseudomonas putida*. J Bacteriol 2008;190:3374–3380.

Pflüger-Grau K, Chavarria M, de Lorenzo V: The interplay of the $EIIA^{Ntr}$ component of the nitrogen-related phosphotransferase system (PTS^{Ntr}) of *Pseudomonas putida* with pyruvate dehydrogenase. Biochim Biophys Acta 2011;1810:995–1005.

Pflüger-Grau K, Görke B: Regulatory roles of the bacterial nitrogen-related phosphotransferase system. Trends Microbiol 2010;18:205–214.

Polarek JW, Williams G, Epstein W: The products of the kdpDE operon are required for expression of the Kdp ATPase of *Escherichia coli*. J Bacteriol 1992;174:2145–2151.

Postma PW, Lengeler JW, Jacobson GR: Phosphoenolpyruvate:carbohydrate phosphotransferase systems of bacteria. Microbiol Rev 1993; 57:543–594.

Powell BS, Court DL, Inada T, Nakamura Y, Michotey V, Cui X, Reizer A, Saier MH, Reizer J: Novel proteins of the phosphotransferase system encoded within the *rpoN* operon of *Escherichia coli* Enzyme IIA^{Ntr} affects growth on organic nitrogen and the conditional lethality of an era^{ts} mutant. J Biol Chem 1995;270: 4822–4839.

Reinsch C: Smoothing by Spline Functions. Berlin, Numerische Mathematik, 1967.

Reizer J, Reizer A, Merrick MJ, Plunkett G, Rose DJ, Saier MH: Novel phosphotransferase-encoding genes revealed by analysis of the *Escherichia coli* genome: a chimeric gene encoding an Enzyme I homologue that possesses a putative sensory transduction domain. Gene 1996;181:103–108.

Schlosser A, Meldorf M, Stumpe S, Bakker EP, Epstein W: TrkH and its homolog, TrkG, determine the specificity and kinetics of cation transport by the Trk system of *Escherichia coli*. J Bacteriol 1995;177:1908–1910.

Silva-Rocha R, Martinez-Garcia E, Calles B, Chavarria M, Arce-Rodriguez A, de las Heras A, Paez-Espino AD, Durante-Rodriguez G, Kim J, Nikel PI, Platero R, de Lorenzo V: The Standard European Vector Architecture (SEVA): a coherent platform for the analysis and deployment of complex prokaryotic phenotypes. Nucleic Acids Res 2013;41:D666–D675.

Velazquez F, Pflüger K, Cases I, De Eugenio LI, de Lorenzo V: The phosphotransferase system formed by PtsP, PtsO, and PtsN proteins controls production of polyhydroxyalkanoates in *Pseudomonas putida*. J Bacteriol 2007;189: 4529–4533.